A Simplified Model for Dynamic Depletion in Doped UTB-SOI/DG-FinFETs

Xing Zhou*, Siau Ben Chiah*, and Li Yuan**

*School of Electrical and Electronic Engineering, Nanyang Technological University
Nanyang Avenue, Singapore 639798, exzhou@ntu.edu.sg
**Institute of Microelectronics, 1 Science Park Road, Singapore Science Park II, Singapore 117685

ABSTRACT

Compact modeling for doped-body MOSFETs, such as ultra-thin body (UTB) SOI and double-gate (DG) FinFETs, represents the most challenging task since it involves the Poisson's solution with two boundary conditions, which is not available when the body doping cannot be ignored. A physically-scalable model in the complete range of operation should capture the surface-potential behaviors in accumulation, depletion, volume-inversion, and strong-inversion regions for any body-doping/thickness variations. It is even more difficult to model the so-called "dynamic depletion" (DD), in which partial to full depletion occurs at the drain end.

In this paper, we extend our unified regional modeling (URM) approach, which has demonstrated scalable depletion to volume-inversion for any body doping/thickness, to modeling the DD effect. The "full-depletion" (FD) condition is reached when the sum of the depletion widths due to the two gates at the source end is equal to the body thickness. The same condition is applied to the drain end, which determines the DD condition. In this way, the FD/DD effects can be modeled by the simple full-depletion approximation. Results of the modeled surface-potential and gate-capacitance are demonstrated with complete scalability over body doping, thickness, and drain voltage, and validated with numerical data.

Keywords: Compact model (CM), double-gate (DG), dynamic-depletion (DD), FinFET, full-depletion (FD), partial-depletion (PD), ultra-thin body (UTB) SOI, unified regional modeling (URM), Xsim.

1 INTRODUCTION

Over half a century, the mainstream CMOS technology has evolved from planar bulk or "partially-depleted" (PD) SOI to vertical double-gate (DG) FinFETs or "fully-depleted" (FD) ultra-thin body (UTB) SOI. Body doping has been, and is still being used as a major means to tune the transistor threshold voltage. Although undoped body has been favored for FinFETs and UTB SOI to reduce random discrete dopant (RDD) fluctuations, body doping may still have to be used in emerging FinFET/UTB-SOI technologies due to required threshold tuning. This poses a major challenge in developing a compact model physically scalable over body doping and body thickness, in which the transistor body can be PD or FD depending on the body doping and thickness as well as the gate bias; or even "dynamically-depleted" (DD) [1]–[3] depending on the drain bias. The difficulty mainly arises due to the fact that the Poisson–Boltzmann equation cannot be integrated twice when the doping term is included while two unknowns for the surface potentials at two gates need to be solved.

The unified regional modeling (URM) approach, as adopted in the development of the Xsim model [4], [5], has demonstrated physical scaling over arbitrary body doping and thickness with PD/FD transitions in generic UTB-SOI/DG-FinFETs. It is based on the simple regional approximation, for which regional depletion and strong-inversion solutions are readily available from bulk-MOS formulations, and the coupling between the two individual gate-controlled formulations is through the "FD condition" when the sum of the two depletion widths is equal to the body thickness.

In this paper, the URM for the surface potential (ϕ_s) with PD/FD transitions at the source end is extended to model the DD effect at the drain end, together with a revised bulk-charge linearization [3] for the bulk-charge factor (A_b), which provides a very simple picture of DD. The simplified DD model is validated in comparison with numerical data of the gate capacitances (C_{gg}) with varying body doping (N_A) and thickness (T_{Si}) at different drain biases.

2 THE SIMPLIFIED DD PICTURE AND MODELING

We consider a symmetric-DG (s-DG) n-FinFET with body doping N_A and thickness T_{Si}. For a UTB-SOI with extremely thick body oxide (BOX), it has similar boundary conditions as those for the half of the symmetric-DG. Under the simple "FD approximation," the depletion width (at a given gate bias V_g) is given by the Poisson solution considering only the N_A term:

$$X_d = \sqrt{\frac{2\varepsilon_{Si}(\phi_s - \phi_o)}{qp_0}} = \sqrt{\frac{2\varepsilon_{Si}}{qp_0}}\left(-\frac{\Upsilon}{2} + \sqrt{\frac{\Upsilon^2}{4} + V_{gf} - \phi_o}\right) \leq \sqrt{\frac{2\varepsilon_{Si}(2\phi_F + V_{cr})}{qp_0}} \equiv X_{dm} \quad (1)$$

where ϕ_s and ϕ_o are the surface and zero-field (ZF) potentials, respectively, and ε_{Si} is the permittivity of Si. $V_{gf} \equiv V_g - V_{FB}$ is the flatband-shifted gate voltage with V_{FB} being the flatband voltage.

$$\Upsilon = \sqrt{2q\varepsilon_{Si} p_0}\,/C_{ox} \tag{1a}$$

is the body factor, in which $C_{ox} = \varepsilon_{ox}/T_{ox}$ is the gate capacitance (per unit area) with T_{ox} being the gate oxide thickness and ε_{ox} being the permittivity of SiO_2.

$$p_0 = n_i e^{\phi_F/v_{th}} = n_i \exp\left[\sinh^{-1}\left(\frac{N_A - N_D}{2n_i}\right)\right] \tag{1b}$$

is the hole concentration at equilibrium (or at flatband), where n_i is the intrinsic carrier concentration and ϕ_F is the Fermi potential, given by the Kingston equation [6]. Υ and p_0 thus defined will be valid for any doping, from heavily-doped to undoped (pure Si) body. $V_{cr} \equiv V_c - V_r$ in (1) is the imref split where V_c is the channel voltage and V_r is the reference voltage, which is equal to V_b for body-contacted (BC) or $\min\{V_s, V_d\}$ for floating-body (FB) devices.

We note that the maximum depletion width X_{dm} defined in (1) is a function of V_c, with $V_s \le V_c(y) \le V_d$ $(0 \le y \le L)$, whereas X_d is a function of V_g only. The *FD voltage* ($V_{g,FD}$) is defined as the gate voltage at which FD occurs, given for s-DG by

$$X_d\left(V_{g,FD}\right) = \sqrt{\frac{2\varepsilon_{Si}}{qp_0}}\left(-\frac{\Upsilon}{2} + \sqrt{\frac{\Upsilon^2}{4} + V_{gf,FD} - \phi_o}\right) = \frac{T_{Si}}{2}, \tag{2}$$

or

$$V_{gf,FD} = \left(\sqrt{\frac{qp_0}{2\varepsilon_{Si}}}\left(\frac{T_{Si}}{2}\right) + \frac{\Upsilon}{2}\right)^2 - \frac{\Upsilon^2}{4}. \tag{2a}$$

For UTB-SOI, the FD condition will be $X_d(V_{g,FD}) = T_{Si}$, and for an independent asymmetric-DG, the FD condition will be $X_{d1}(V_{g1,FD}) + X_{d2}(V_{g2,FD}) = T_{Si}$. The corresponding *FD potential* is given by

$$\phi_{FD} = \phi_s - \phi_o = \frac{qp_0 X_d^2\left(V_{g,FD}\right)}{2\varepsilon_{Si}} = \left(-\frac{\Upsilon}{2} + \sqrt{\frac{\Upsilon^2}{4} + V_{gf,FD} - \phi_o}\right)^2. \tag{3}$$

The *ZF location*, at which $d\phi/dx = 0$, is defined as $X_{o,c} = \min\{X_d(V_{g,FD}), X_{dm}(V_c)\}$ $(c = s, d)$. Now, we can define three cases for s-DG FinFETs at a given $V_{ds} > 0$: (i) PD: $X_{dm}(V_d) < T_{Si}/2$ (i.e., whole body always PD), (ii) FD: $X_{dm}(V_s) > T_{Si}/2$ (i.e., whole body has PD/FD transition), and (iii) DD: $X_{dm}(V_s) < T_{Si}/2$ and $X_{dm}(V_d) > T_{Si}/2$ (i.e., source end always PD and drain end has PD/FD transition). This is illustrated in Fig. 1 for the FinFETs with $N_A = 10^{18}$ cm^{-3} and three body thicknesses, $T_{Si} = 20$, 90, and 150 nm, biased at $V_{ds} = 1.2$ V. Similar ones can be drawn for FinFETs with different body doping for the same body thickness.

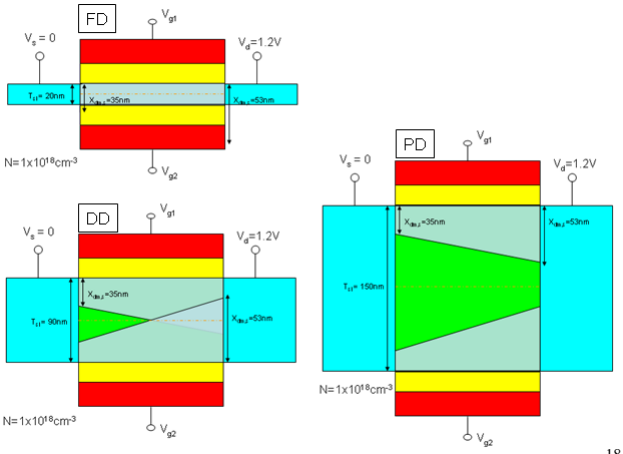

Figure 1: Schematic illustration of s-DG FinFETs with $N_A = 10^{18}$ cm^{-3} and $T_{Si} = 20$, 90, and 150 nm as well as calculated X_{dm} at $V_{ds} = 1.2$ V, under PD (*right*), FD (*upper-left*), and DD (*lower-left*) operations.

The aforementioned simple picture based on the FD approximation has been successfully applied to model the PD/FD cases by our URM model [4], [5], which is based on the symmetric bulk-charge linearization [7], with the bulk-charge factor given by

$$\overline{A_b} \equiv -\left.\frac{\partial q_i}{\partial \phi_s}\right|_{\phi_s = \overline{\phi_s}} = 1 + \frac{\Upsilon}{2\sqrt{\overline{\phi_s} - \overline{\phi_o}}}, \tag{4}$$

$$q_i = V_{gf} - \phi_s - \Upsilon\sqrt{\phi_s - \phi_o}, \tag{4a}$$

$$\overline{\phi_s} = \left(\phi_{s,s} + \phi_{s,d}\right)/2. \tag{4b}$$

(4) is valid for PD (similar to bulk) and FD where the bulk charge is fixed (y independent). However, it is no longer suitable for DD with y-dependent bulk-charge variations.

Following the approach to symmetric linearization for DD [3] and combining with our URM for the single-piece surface potential, ϕ_{ds}, from depletion to strong inversion [4], [5], a revised bulk-charge factor is modeled by

$$\overline{A_{b,DD}} \equiv -\frac{\Delta q_i}{\Delta \phi_{ds}} = \frac{q_{i,s} - q_{i,d}}{\phi_{ds,d} - \phi_{ds,s}}, \tag{5}$$

$$q_{i,d} = \vartheta_f\left(V_{gf}; \sigma_f\right) - \phi_{ds,d} - \Upsilon\sqrt{\phi_{ds,d} - \phi_{o,d}}, \tag{5a}$$

$$q_{i,s} = \vartheta_f\left(V_{gf}; \sigma_f\right) - \phi_{ds,s} - \Upsilon\sqrt{\phi_{ds,s} - \phi_{o,s}}, \tag{5b}$$

$$\vartheta_f\{x;\sigma\} = 0.5\left(x + \sqrt{x^2 + 4\sigma}\right). \tag{5c}$$

Due to the use of ϕ_{ds} and the "forward smoothing function" for V_{gf}, no singularity occurs at flatband. The surface

potential and charges crossing the flatband and in accumulation are modeled together with the ϕ_{acc} regional solution. All other formulations follow the URM (Xsim) [4], [5].

For reference, the unified regional surface-potential equations are listed below.

$$\phi_s = \begin{cases} \phi_{acc} = \vartheta_r\left(V_{gf};\sigma_a\right) + 2v_{th}\mathcal{L}\left\{\dfrac{\Upsilon}{2\sqrt{v_{th}}}e^{-\left(V_{gf}-V_r\right)/2v_{th}}\right\} \\ \phi_{sub} = \phi_o + \left(-\dfrac{\Upsilon}{2} + \sqrt{\dfrac{\Upsilon^2}{4} + \vartheta_f\left(V_{gf}-\phi_o;\sigma_f\right)}\right)^2 \\ \phi_{dep} = \vartheta_{eff}\left(\phi_{sub},\phi_{FD};\delta_d\right) \\ \phi_{dv} = V_{gf} - \Upsilon\sqrt{\phi_{dep}} \\ \phi_{str} = \vartheta_f\left(V_{gf};\sigma_s\right) - 2v_{th}\mathcal{L}\left\{\dfrac{\Upsilon}{2\sqrt{v_{th}}}e^{\left(V_{gf}-2\phi_F-V_c\right)/2v_{th}}\right\} \\ \phi_{ds} = \vartheta_{eff}\left(\phi_{dv},\phi_{str};\delta_\phi\right) \end{cases} \tag{6}$$

$$\vartheta_r\left\{x;\sigma\right\} = 0.5\left(x - \sqrt{x^2+4\sigma}\right), \tag{6a}$$

$$\vartheta_{eff}\left\{x, x_{sat};\delta\right\} = x_{sat} - 0.5\left[x_{sat} - x - \delta + \sqrt{\left(x_{sat}-x-\delta\right)^2 + 4\delta x_{sat}}\right] \tag{6b}$$

where $\mathcal{L}\{W\}$ is the *Lambert W* function and $v_{th} = kT/q$ is the thermal voltage. The terminal-charge models [5], with $A_{b,DD}$ replacing A_b, are listed below.

$$\begin{cases} Q_b = -C_{ox}\left[q_{b,acc} + q_{b,sub} - \dfrac{\left(\overline{A_{b,DD}}-1\right)\Delta\phi_{ds}^2}{12H_{DD}}\right] \\ Q_d = -\dfrac{C_{ox}}{2}\left[\overline{q_i} - \dfrac{\overline{A_{b,DD}}\Delta\phi_{ds}}{6}\left(1 - \dfrac{\Delta\phi_{ds}}{2H_{DD}} - \dfrac{\Delta\phi_{ds}^2}{20H_{DD}^2}\right)\right] \\ Q_s = -\dfrac{C_{ox}}{2}\left[\overline{q_i} + \dfrac{\overline{A_{b,DD}}\Delta\phi_{ds}}{6}\left(1 + \dfrac{\Delta\phi_{ds}}{2H_{DD}} - \dfrac{\Delta\phi_{ds}^2}{20H_{DD}^2}\right)\right] \end{cases} \tag{7}$$

$$q_{b,acc} = \vartheta_r\left(V_{gf};\sigma_a\right) - \phi_{acc}, \tag{7a}$$

$$q_{b,sub} = \vartheta_f\left(V_{gf};\sigma_a\right) - \vartheta_f\left(V_{gf};\sigma_f\right) + \Upsilon\sqrt{\overline{\phi_{ds}} - \overline{\phi_o}}, \tag{7b}$$

$$H_{DD} = \left(\overline{q_i}/\overline{A_{b,DD}}\right) + v_{th}. \tag{7c}$$

It will be shown in the next section that with only the revised bulk-charge factor in (5), our URM approach can capture the DD as well as PD/FD behaviors in C_{gg}, scalable for any terminal biases as well as body doping and thickness variations.

3 RESULTS AND DISCUSSION

The simple picture for capturing the DD effect is shown through two examples of long-channel ($L = 10$ μm) FinFETs. In the first one, four body thicknesses with the same body doping of $N_A = 1\times10^{18}$ cm^{-3} are compared. ϕ_{ds} based on (6) are calculated for $V_c = 0$ and 1.2 V as a function of V_g, as shown in Fig. 2, and the corresponding FD voltages based on (2a) are labeled for the 4 devices. It can be seen that it is always PD ($\phi_{ds} \sim \phi_{sub}$) for $T_{Si} = 150$ nm whereas it is always FD ($\phi_{ds} \sim \phi_{dv}$) for $T_{Si} = 20$ nm. For the $T_{Si} = 60$-nm FinFET, the source-end ($\phi_{ds,s}$ with $V_c = 0$) becomes FD at $V_{g,FD} = 0.23$ V, beyond which it is always FD regardless of V_{ds}. This has been modeled by our previous URM [4], [5] with the bulk-charge factor given by (4). However, when $T_{Si} = 90$ nm, FD voltage is $V_{g,FD} = 1.33$ V and the source-end never becomes FD (since $X_{dm,s} < T_{Si}/2$). Then, DD occurs as long as $2\phi_F + V_d > \phi_{FD}$ in (3), which is modeled *consistently* in our URM, with the bulk-charge factor being modeled by (5).

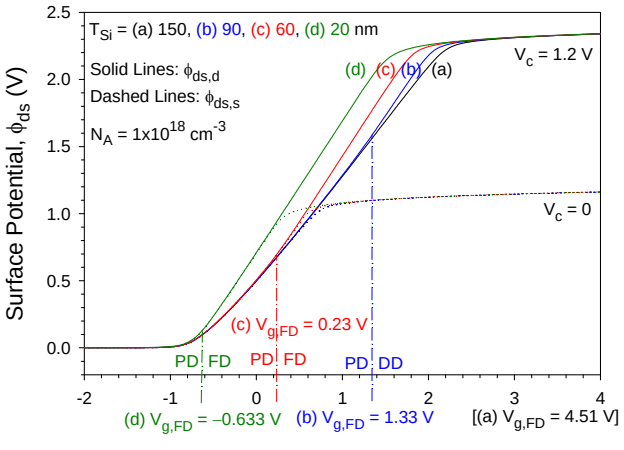

Figure 2: ϕ_{ds} vs. V_g at $V_c = 0$ and 1.2 V for FinFETs with T_{Si} = (a) 150, (b) 90, (c) 60, and (d) 20 nm, all with $N_A = 10^{18}$ cm^{-3}.

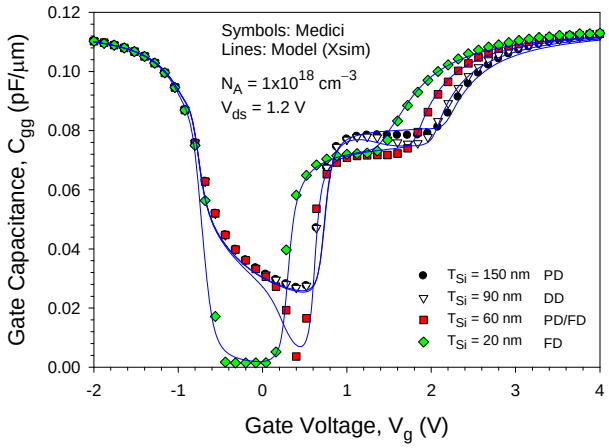

Figure 3: Modeled (*lines*) and numerical (*symbols*) C_{gg} vs. V_g at $V_{ds} = 1.2$ V for FinFETs with $T_{Si} = 150$, 90, 60, and 20 nm, all with $N_A = 10^{18}$ cm^{-3}.

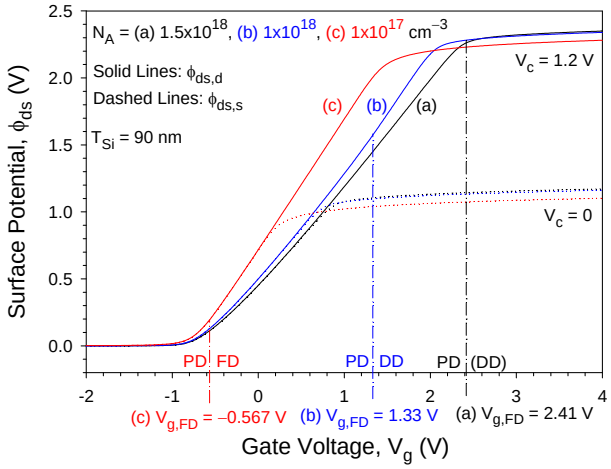

Figure 4: ϕ_{ds} vs. V_g at $V_c = 0$ and 1.2 V for FinFETs with N_A = (a) 1.5×10^{18}, (b) 1×10^{18}, and (c) 1×10^{17} cm^{-3}, all with $T_{Si} = 90$ nm.

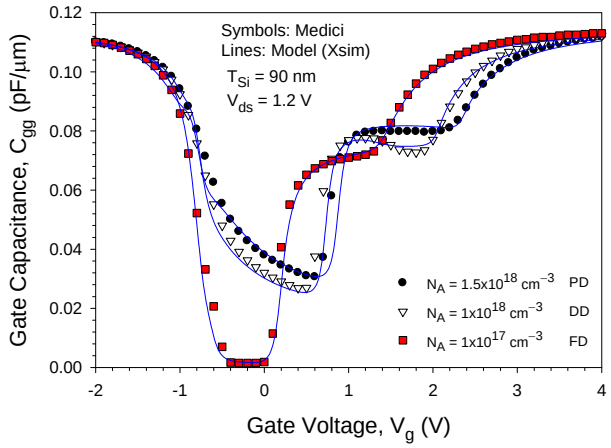

Figure 5: Modeled (*lines*) and numerical (*symbols*) C_{gg} vs. V_g at $V_{ds} = 1.2$ V for FinFETs with $N_A = 1.5\times10^{18}$, 1×10^{18}, and 1×10^{17} cm^{-3}, all with $T_{Si} = 90$ nm.

The aforementioned ϕ_{ds} model, combined with the regional ϕ_{acc} and terminal-charge models, for PD-FD-DD effects with varying body thickness is validated in comparison with the same (ideal) numerical devices, as shown in Fig. 3 for the C_{gg} vs. V_g of the 4 FinFETs. The DD effect, as shown by the decrease in C_{gg} with increasing $V_g > V_{g,FD}$, for the $T_{Si} = 90$-nm FinFET (*triangle*) is clearly captured physically. Equation (5) for the bulk-charge factor is used for all the models.

The second example shows three FinFETs with varying body doping of $N_A = 1.5\times10^{18}$, 1×10^{18}, and 1×10^{17} cm^{-3} with the same $T_{Si} = 90$ nm. ϕ_{ds} are calculated for $V_c = 0$ and 1.2 V, as shown in Fig. 4, with the corresponding FD voltages labeled. The FinFET becomes DD when $N_A = 1\times10^{18}$ cm^{-3}, but it is always FD when $N_A = 1\times10^{17}$ cm^{-3} (except for $V_g < -0.567$ V). However, it will always be PD if $N_A \geq 1.5\times10^{18}$ cm^{-3}, unless the operating voltage ($V_{dd} = 1.2$ V) is increased, for which DD may occur. Similarly, these three device C_{gg} characteristics have been validated by comparison with numerical data, as shown in Fig. 5.

4 SUMMARY AND CONCLUSIONS

The dynamic-depletion effect in a generic DG MOSFET, one of the most challenging tasks in compact modeling, has been modeled by the simple full-depletion picture in which the FD condition occurs when the sum of the individual depletion widths by the two gates is equal to the body thickness while the maximum depletion widths are evaluated at the source and drain ends, respectively. For a given $V_{ds} > 0$, if the FD potential ϕ_{FD} is in between $2\phi_F + V_s$ and $2\phi_F + V_d$, DD occurs; otherwise, only FD occurs if $\phi_{FD} < 2\phi_F + V_s$, or only PD occurs if $\phi_{FD} > 2\phi_F + V_d$.

The simplified model for the DD effect with a modified bulk-charge factor is made possible by the URM approach, in which physical regional solutions govern the device operations in their respective regions. The transition from PD to FD in the subthreshold region modeled by the source-end $\phi_{ds,s}$ through the transition from ϕ_{sub} to ϕ_{dv}, respectively, is extended to the PD-to-DD transition in the saturation region modeled by the drain-end $\phi_{ds,d}$ in the same way. Physical parameter scalability is built into the model.

Acknowledgement: This work was supported in part by the Institute of Microelectronics under Agreement for Research Collaboration through the A*STAR SERC Grant No. 102 165 0085.

REFERENCES

[1] D. Sinitsky, S. Fung, S. Tang, P. Su, M. Chan, P. Ko, and C. Hu, "A dynamic depletion SOI MOSFET model for SPICE," in *1998 VLSI Tech. Dig.*, pp. 114–115.

[2] J. Zhang, L. Zhang, J. He, and M. Chan, "A noncharge-sheet channel potential and drain current model for dynamic-depletion silicon-on-insulator metal-oxide-semiconductor field-effect transistors," *J. Appl. Phys.*, vol. 107, 054507, 2010.

[3] W. Wu, W. Yao, and G. Gildenblat, "Surface-potential-based compact modeling of dynamically depleted SOI MOSFETs," vol. 54, pp. 595–604, 2010.

[4] X. Zhou, "Xsim: A unified compact model for bulk/SOI/DG/GAA MOSFETs," in *Proc. WCM-Nanotech 2011*, Jun. 2011, vol. 2, pp. 726–731.

[5] X. Zhou, G. J. Zhu, G. H. See, K. Chandrasekaran, S. B. Chiah, and K. Y. Lim "Unification of MOS compact models with the unified regional modeling approach," *J. Comput. Electron.*, vol. 10, no. 1, pp. 121–135, Mar. 2011.

[6] R. H. Kingston and S. F. Neustadter, "Calculation of the space charge, electric field, and free carrier concentration at the surface of a semiconductor," *J. Appl. Phys.*, vol. 26, no. 6, pp. 718–720, Jun. 1955.

[7] T. L. Chen and G. Gildenblat, "Symmetric bulk charge linearization in charge-sheet MOSFET model," *Electron. Lett.*, vol. 37, no. 12, pp. 791–793, Jun. 2001.